Adhesion of heterogeneous thin films—I: Elastic heterogeneity

S.M. Xia [a,*], L. Ponson [b], G. Ravichandran [c], K. Bhattacharya [c]

[a] Woodruff School of Mechanical Engineering, Georgia Institute of Technology, Atlanta, GA 30332, USA
[b] Institut de Mcanique d'Alembert, Universit Pierre et Marie Curie, F-75005 Paris, France
[c] Division of Engineering and Applied Science, California Institute of Technology, Pasadena, CA 91125, USA

ABSTRACT

We study the adhesion of thin films on rigid substrates in the presence of spatial hetero-geneities. While adhesion is relatively well-understood in the context of homogeneous systems, much remains open concerning the adhesion of heterogeneous systems. In this paper, we focus on thin adhesive tape with heterogeneities in the elastic stiffness, and show that these heterogeneities have a profound effect on adhesion raising the effective force required to peel the film by an order of magnitude with no modification of the actual adhesive interface. We show through theory and experiment that this apparent increase is caused by fluctuations in the elastic bending energy. We also show that heterogeneities can be used to create asymmetry in that the force required to peel the tape in one direction can be different from that in the other. In short, this work shows that fluctuations in a small component of the overall energy of the system can give rise to a significant macroscopic consequence. We comment on the broader implications of this observation.

© 2012 Elsevier Ltd. All rights reserved.

1. Introduction

Virtually all engineering materials are heterogeneous on a fine scale: alloys and ceramics are polycrystalline, while polymers and glasses often have fluctuations in density and composition. Composite materials are heterogeneous by design, and heterogeneous materials are ubiquitous in nature. These heterogeneities affect the properties of the material at the macroscopic scale, and understanding this link between heterogeneous microstructure and overall or effective properties is a topic of vital importance. There is by now a well-developed theory that describes the overall or effective properties of heterogeneous materials in the context of elasticity, electrostatics, magnetism and other properties that are characterized by minimum energy principles (e.g., Milton, 2002; Nemat-Nasser and Hori, 1999). Some of these methods have been extended to dissipative processes like plasticity, but these methods work best in the context of deformation theory which one can formulate as a minimum energy principle.

However, the understanding of effective properties remains incomplete in the context of time or history-dependent phenomena. This is especially so in the context of free-boundary and free-discontinuity problems like adhesion, fracture, and phase transformations. The key difficulty is that bounds on the energy do not necessarily imply bounds on the derivatives of the energy; a small bump in the energy landscape can become a very large bump in the forcing leading to a significant effect on the overall properties.

In this work, we explore this issue in the context of the peeling of adhesive tape. This is a well-understood phenomenon in homogeneous materials going back to the discerning work of Rivlin (1944) that related the force required to peel an

---

adhesive film from a rigid substrate to the adhesive energy of the interface. We show that heterogeneity brings a number of surprises. In this paper, we study the consequences of making the elastic properties of the tape heterogeneous; we show that we can dramatically increase the 'stickiness' (effective adhesive energy or adhesion strength) of the tape by introducing elastic heterogeneity even though we do not modify the actual adhesive surface in any way. This is closely related to the insightful work of Kendall (1975a). We also show that elastic heterogeneity can be used to create asymmetry where the adhesive force required to peel the tape in one direction is different from that in the other. In subsequent works, we address the consequences of spatial heterogeneity in adhesive properties (Xia et al., 2012a; Ponson and Xia, 2012). A summary of all these results was announced in Xia et al. (2012b).

Adhesion of thin films not only provides an idealized context to study broad questions, but is of inherent scientific and technological interest. Thin-film structures are prevalent in many physical, engineering, and biological systems, such as photovoltaic panels, integrated circuits, flexible electronics, packing tapes, gecko setae, to name just a few. In these systems, strong interfacial bonding between films and their bases is often desirable to ensure system integrity and reliability. The physical origin of interfacial bonding may include covalent and ionic atomic bonding, van der Walls interaction, electrostatic forces, or any of these in combination. Irrespective of the actual mechanism, the bonding strength or toughness of an interface can be quantified by adhesion energy, which is defined as the amount of energy required to fracture a unit area of the interface.

A vast body of research has been conducted for increasing adhesion energies of various bi-material interfaces through modification of interfacial chemical bonding (e.g., Hirsch and Varga, 1978; Fowkes, 1987; Liu et al., 1996; Hudaa et al., 2008). Such intrinsic mechanisms of interfacial strengthening are usually material-specific, and rarely transferable to other material systems. So more mechanistic approaches have been considered recognizing the fact that peeling involves the nucleation and propagation of the peel front. In particular, the use of interfacial roughness to increase the fracture toughness of bi-material interfaces (e.g., Evans and Hutchinson, 1989; Guduru, 2007; Guduru and Bull, 2007; Zavattieri et al., 2007; Reedy, 2008; Li and Kim, 2009) has been extensively studied. This points to the role of heterogeneities.

The role of heterogeneities was highlighted in the insightful work of Kendall (1975a). He fabricated rubber tape with alternating stiffness by either introducing reinforcement or changing thickness in alternating segments, adhered it to glass and peeled it at a constant peeling force. He observed that the peel front slowed down as it approached a reinforced or thicker segment. He developed a model that suggested these were a result of the abrupt change in bending stiffness and this abrupt change would result in an enhancement of overall adhesive strength by a factor equal to the ratio of bending stiffness.

In a variation of this work, Ghatak et al. (2004) studied the process of peeling of a flexible, but stiff, plate from a thin patterned adhesive elastic layer. They found that the initiation of the crack on a patterned tape occurs at much higher loads than that required on a smooth adhesive layer. Chung and Chaudhury (2005) made similar observations with significant toughening and attributed it to sequential crack nucleation at tough local heterogeneities. Similar studies were conducted by Ramrus and Berg (2006) and Chan et al. (2007), and an analysis emphasizing crack pinning was reported by Dalmas et al. (2009). Chen et al. (2008, 2009) also investigated the apparent fracture/adhesion energy of an interface with periodic cohesive interactions, and showed that this energy can be tailored between the average and the peak value of the local cohesive energy by controlling the ratio of the period of cohesive energy to the cohesive zone size.

There is a related, and much larger literature, on fracture of heterogeneous solids. Many of these are motivated by ceramics and composites, where microstructural features have been exploited to enhance the toughness (e.g., Bower and Ortiz, 1991, 1993; Hutchinson and Suo, 1992; Xu et al., 1998; Cox and Yang, 2006, and references there). Others are motivated by nature which has exploited microstructure to enhance toughness of nacre and other shells (e.g., Menig et al., 2000; Barthelat and Espinosa, 2007, and references there). Recently, random variations of fracture energy at the microscale have been considered and their effect on macroscopic failure properties, such as morphology of fracture surfaces and crack kinetics, has been investigated. It was shown that these systems can be described by universal scaling laws (Bouchaud, 1997; Bonamy et al., 2008; Ponson and Bonamy, 2010).

In the current work, we revisit the work of Kendall (1975a). We study the process of peeling a tape with heterogeneous bending stiffness but with uniform adhesive strength. Specifically, we make a tape with varying bending stiffness and peel it at a fixed angle and at a constant velocity. We observe a significant increase both in the force and the work required to peel a macroscopic length of tape. We analyze the problem theoretically by considering the tape to be an inextensible Euler–Bernoulli beam with heterogeneous stiffness. We find good agreement between theory and experiment, and thereby establish that the enhanced adhesive force and energy are indeed the result of the bending heterogeneity. In particular, as the peel front goes from a compliant to a stiff segment, much of the work done by the applied force goes into bending the suddenly stiff tape and a larger applied force is required to propagate the peel front. Our analysis provides concrete predictions about the enhancement and how it depends on contrast, peeling angle, and length scales. Our analysis also shows that the adhesion can be asymmetric, in the sense that the maximum peel force required to peel the tape from one end can be different from that required to peel the same tape from the other.

In Section 2, we describe a theoretical model for predicting the peeling response of a discretely heterogeneous film via a variational approach. Analytic solutions in a few special cases are presented first, followed by a numerical scheme for handling the general case. Section 3 covers the experimental construction of a model material system and a peel-test setup. Theoretical and experimental results from a systematic parametric study are presented in Section 4. Finally, we discuss the implications and limitations of our findings in Sections 5.

2. Theory

Fig. 1 is a schematic diagram of an elastically heterogeneous film or strip under consideration. The film is composed of N segments, each of which is homogeneous, but has generally different bending rigidities, $D_i = E_i^* I_i$ ($1 \leq i \leq N$). Here E_i^* is the reduced elastic modulus ($E_i/(1-v_i^2)$) and I_i is the second moment of cross-sectional area. Heterogeneity in D_i can arise from differences in E_i^*, or I_i, or both. We assume that the film is inextensible, and this is known to be a good assumption at moderate to large peel angle (Kendall, 1975b). The profile of the inextensible film is uniquely described by a function of $\theta(s)$, where s is the arc-length along the film with respect to the origin O and θ is the inclination angle between the film tangent and the horizontal plane. The discontinuities of bending rigidity are located at $s = s_i$ with inclination angles of θ_i. The film is perfectly bonded to the rigid substrate up to some arc-length l, and is being peeled off at a peel angle under a peel force, $\overrightarrow{F}$, which makes an angle θ_p with respect to the horizontal. Therefore, we have boundary conditions

$$\theta(l) = 0, \quad \theta'(s_N^-) = 0. \tag{1}$$

The second boundary condition reflects the fact that there is no applied moment at s_N. For convenience of notation we set $s_0 = l$.

The potential energy of the system is

$$\mathcal{E} = \int_l^{s_N} \frac{1}{2} D(s)(\theta'(s))^2 \, ds - \overrightarrow{F} \cdot \overrightarrow{u}_p - \int_0^l G \, ds, \tag{2}$$

where $\overrightarrow{u}_p$ is the displacement of the point of application of the force ($s = s_N$), $D(s)$ is the distribution of bending rigidity, $\theta'(s)$ is the curvature of the film, and G is the constant adhesion energy (per unit length so that it is adhesion energy per unit area times the width of the film) between the film and the substrate. We express the peel displacement in terms of the distribution of inclination angle as

$$\overrightarrow{u}_p = \int_0^{s_N} \begin{pmatrix} \cos\theta - \cos\theta_p \\ \sin\theta - \sin\theta_p \end{pmatrix} ds. \tag{3}$$

This displacement is measured relative to a reference position at

$$\begin{pmatrix} s_N \cos\theta_p \\ s_N \sin\theta_p \end{pmatrix}.$$

Note that the subtraction in the integrand ensures convergence of $\overrightarrow{u}_p$ when $s_N \to \infty$. Substitution of the expression of $\overrightarrow{u}_p$, together with

$$\overrightarrow{F} = F \begin{pmatrix} \cos\theta_p \\ \sin\theta_p \end{pmatrix}$$

and $D(s) = D_i$ ($s_{i-1} < s < s_i$), into Eq. (2) yields

$$\mathcal{E} = \sum_{i=1}^N \int_{s_{i-1}}^{s_i} \frac{1}{2} D_i(\theta'(s))^2 \, ds - \int_0^{s_N} F(\cos(\theta - \theta_p) - 1) \, ds - \int_0^l G \, ds. \tag{4}$$
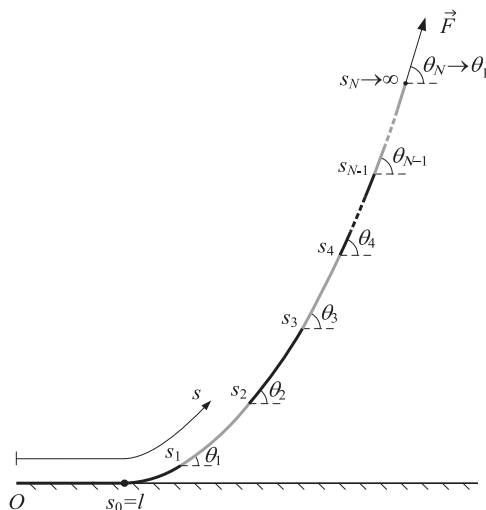
Fig. 1. Peeling of an elastically heterogeneous thin film from a rigid substrate.

To find the equilibrium profile and peel-front position, we take the first variation of the potential energy with respect to the θ subject to boundary conditions (1) and with respect to l. We obtain

$$\delta\mathcal{E} = -\frac{1}{2}D_1(\theta'|_{l+})^2\,\delta l + \sum_{i=1}^{N}\left(D_i(\theta'\,\delta\theta)\Big|_{s_{i-1}}^{s_i} - \int_{s_{i-1}}^{s_i}D_i\theta''\delta\theta\,ds\right) + \int_0^{s_N}F\sin(\theta-\theta_p)\,\delta\theta\,ds - G\,\delta l. \tag{5}$$

By taking a variation of the first of the boundary conditions (1), we obtain the compatibility condition $\delta(\theta|_{l+}) = (\delta\theta)|_{l+} + \theta'|_{l+}\,\delta l = 0$. We insert this into Eq. (5) and rearrange terms to obtain

$$\delta\mathcal{E} = -\sum_{i=1}^{N}\int_{s_{i-1}}^{s_i}\{D_i\theta''-F\sin(\theta-\theta_p)\}\,\delta\theta\,ds + \sum_{i=1}^{N-1}\left(D_i\theta'|_{s_i^-} - D_{i+1}\theta'|_{s_i^+}\right)(\delta\theta)|_{s_i}$$

$$+F\theta'|_{s_N^-}(\delta\theta)|_{s_N} + \left(\frac{1}{2}D_1\theta'^2|_{l+} - G\right)\delta l. \tag{6}$$

For equilibrium and quasi-static processes, the first variation has to vanish for all possible δl and $\delta\theta$ consistent with boundary conditions. Therefore, we conclude

$$D_i\theta'' - F\sin(\theta-\theta_p) = 0 \quad \text{for } s_{i-1} < s < s_i, \; 1 \le i \le N, \tag{7}$$

$$D_i\theta'|_{s_i^-} - D_{i+1}\theta'|_{s_i^+} = 0 \quad \text{for } 1 \le i \le N-1, \tag{8}$$

$$\theta'|_{s_N^-} = 0, \tag{9}$$

$$\tfrac{1}{2}D_1\theta'^2|_{l+} - G = 0. \tag{10}$$

The physical meaning of the above equalities is obvious: Eq. (7) is the equilibrium equation for each segment of the film, Eq. (8) indicates that the bending moment is continuous at $s = s_i$, Eq. (9) reproduces the natural boundary condition of zero moment at the end, and Eq. (10) gives the crack nucleation criterion at the peel front. To these we append the boundary and continuity conditions

$$\theta(l) = 0, \tag{11}$$

$$\theta(s_i^-) = \theta(s_i^+), \quad 1 \le i \le N-1. \tag{12}$$

Eq. (7) subject to Eqs. (8), (9), (11), and (12) determines the shape of the film while Eq. (10) may be regarded as the criterion for the propagation of the peel front and gives the relation between G and F at equilibrium.

While solving the non-linear equation (7) is difficult, it is possible to integrate it once to obtain some interesting insights. Multiplying Eq. (7) by $D_i\theta'$, and integrating from s_0 to s_N, we get

$$\sum_{i=1}^{N}\left\{\frac{1}{2}D_i^2\left((\theta'|s_{i-1}^+)^2 - (\theta'|s_i^-)^2\right) - FD_i(\cos(\theta_i-\theta_p) - \cos(\theta_{i-1}-\theta_p))\right\} = 0. \tag{13}$$

Multiplying the jump condition (8) with $D_i\theta'|_{s_i^-} + D_{i+1}\theta'|_{s_i^+}$, we conclude that $(D_i\theta'|_{s_i^-})^2 = (D_{i+1}\theta'|_{s_i^+})^2$. We can use this to simplify the first term in the sum to obtain

$$\frac{1}{2}D_1^2(\theta'|s_0^+) - \frac{1}{2}D_N^2(\theta'|s_N^-) - F\sum_{i=1}^{N}D_i(\cos(\theta_i-\theta_p) - \cos(\theta_{i-1}-\theta_p)) = 0. \tag{14}$$

Use the propagation equation (10) to rewrite the first term as D_1G, note that the second term is zero due to the boundary condition (9) and set $f(\alpha,\beta) = \cos(\alpha-\theta_p) - \cos(\beta-\theta_p)$. We obtain a relation between the peel force, the adhesion energy and the angles at the interfaces

$$F = \frac{D_1G}{\sum_{i=1}^{N}D_if(\theta_i,\theta_{i-1})}. \tag{15}$$

Similarly, we again multiply Eq. (7) by $D_i\theta'$ but now integrate from s_0 to s where $s_{k-1} \le s \le s_k$ $(1 \le k \le N)$. We again use the jump condition (8) and propagation equation (10) to conclude

$$\frac{1}{2}D_1^2(\theta'|s_0^+) - \frac{1}{2}D_k^2(\theta'(s)) - F\sum_{i=1}^{k-1}D_if(\theta_i,\theta_{i-1}) - FD_kf(\theta,\theta_{k-1}) = 0. \tag{16}$$

Invoking the propagation criterion (10) to rewrite the first term and solving from $\theta'(s)$, we conclude

$$\frac{d\theta}{ds} = \frac{\sqrt{2}}{D_k}\sqrt{D_1G - F\left\{\sum_{i=1}^{k-1}D_if(\theta_i,\theta_{i-1}) + D_kf(\theta,\theta_{k-1})\right\}}. \tag{17}$$

The right-hand side of Eq. (17) only involves the variable θ. Further, it is non-negative. Therefore, we can integrate this equation (formally move it to the left side and ds to the right side) to obtain

$$\int_{\theta_{k-1}}^{\theta_k} \frac{d\theta}{\sqrt{D_1 G - F\left\{\sum_{i=1}^{k-1} D_i f(\theta_i, \theta_{i-1}) + D_k f(\theta, \theta_{k-1})\right\}}} = \frac{\sqrt{2}}{D_k}(s_k - s_{k-1}). \tag{18}$$

Eqs. (15) and (18) are $N+1$ non-linear equations with $N+1$ unknowns of F and θ_k ($1 \leq k \leq N$). Generally, these equations have to be solved numerically to obtain the unknowns. However, analytical solutions are available under certain special circumstances. In the rest of this section, we will gain some valuable insight into the problem by discussing a few special cases, and finish by presenting an iterative numerical procedure which can be employed to handle the general case.

2.1. Homogeneous film

The film has uniform rigidity and therefore consists of only one segment with ends at s_0 and s_1. We first show that as this strip becomes very long ($s_1 \to \infty$), the end angle θ_1 approaches the angle θ_p of applied force. To this end, note that Eqs. (18) and (15) become

$$F = \frac{G}{f(\theta_1, 0)}, \quad \int_0^{\theta_1} \frac{d\theta}{\sqrt{D_1 G - F f(\theta, 0)}} = \frac{\sqrt{2}}{D_1}(s_1 - s_0). \tag{19}$$

Substituting the former in the latter and recalling the definition of f, we obtain

$$\int_0^{\theta_1} \frac{d\theta}{\sqrt{\cos(\theta_1 - \theta_p) - \cos(\theta - \theta_p)}} = \sqrt{\frac{2F}{D_1}}(s_1 - s_0). \tag{20}$$

This is a equation for θ_1. We can show that the left-hand side is a monotonically increasing function of θ_1 with limits of 0 and ∞ as θ_1 goes from 0 to θ_p, respectively. Therefore, there is a unique solution θ_1 as a function of the length ($s_1 - s_0$). Further, if the length of the strip is large compared to $\sqrt{D_1/2F}$, then it follows that $\theta_1 \to \theta_p$.

In any case, returning to our case of long homogeneous strip, we see on substituting $\theta_1 = \theta_p$ in Eq. (19)$_1$ that

$$F_{\text{Hom}} = \frac{G}{1 - \cos \theta_p}, \tag{21}$$

which is the well-known result of Rivlin (1944). Eq. (21) indicates that the peel force in the homogeneous case is only dependent on the adhesion energy and the peel angle, and is irrelevant to other material and geometrical properties of the film.

Note that the argument above (Eq. (20)) alerts us that an important length scale in the problem is $\sqrt{D/2F}$: it is the length of film of stiffness D that suffers bending under an applied load F. However, it is somewhat inconvenient to directly use this length scale. In what follows, we consider the case where D varies and consequently F as we shall see. Further, F is a part of the answer that we seek to compute. However, F is proportional to G (cf. Eq. (21)), and G is constant by assumption in this work. So, from now on, we shall use $\lambda = \sqrt{D_e/2G}$ as the characteristic length scale where D_e is a representative rigidity.

2.2. Two-segment heterogeneous film

Consider a heterogeneous film comprising of two segments ($N=2$) with different bending rigidities, D_1 and D_2. The discontinuity of bending rigidity occurs at $\theta = \theta_1$. We assume that the strip is long compared to $\lambda = \sqrt{D_e/2G}$ so that $\theta_2 = \theta_p$. From Eq. (15), we find the peel force to be

$$F_{\text{Het}} = \frac{GD_1}{D_2 + (D_2 - D_1)\cos(\theta_1 - \theta_p) - \cos(\theta_p)}. \tag{22}$$

The peeling force depends on θ_1 which in turn depends on the position s_1 of the interface. So the force required to peel this tape depends on the maximum value of the peeling force. This occurs when $D_1 > D_2$, i.e., when the adhered portion of the film has a higher bending rigidity, and for $\theta_1 = 0$:

$$F_{\text{Het}}^{2\text{seg}} = \frac{D_1 G}{D_2(1 - \cos(\theta_p))} = \frac{D_1}{D_2} F_{\text{Hom}}. \tag{23}$$

In other words, the force required to peel this two-segment film is higher than that of the homogeneous film, and the enhancement ratio is D_1/D_2 independent of the peel angle and the intrinsic adhesion energy.

2.3. Periodically heterogeneous film

Consider a periodically heterogeneous film with period p where each period is made of M segments of bending rigidity $D^{(j)}$ and length fraction $\chi^{(j)}, j = 1, \ldots, M$. We use the superscript in parenthesis (j) for local indexing within each period, and

the superscript (k,j) to denote the j-th segment in k-th period (unit cell). We shall show that the overall behavior of the film depends sensitively on the ratio between the period and the length scale of bending ($\sqrt{D_e/2G}$ where we take D_e as a representative rigidity). We treat the two asymptotic cases, the period very small compared to this length scale and the period very large compared to this length scale analytically and show using numerics that the general case bridges these two limits.

2.3.1. Small period ($p \ll \sqrt{D_e/2G}$)

Recall from the general setting that the angle between two adjoining interfaces is given by Eq. (18). We observe that the integrand is bounded away from zero independent of k, and it follows that $(\theta_k - \theta_{k-1}) \to 0$ and $(s_k - s_{k-1}) \to 0$ uniformly in k. In our periodic setting, we have $\Delta\theta = \max_{k,j} \Delta\theta^{(k,j)} = \max_{k,j} \theta^{(k,j)} - \theta^{(k,j-1)} = O(p)$. It is shown in the appendix that, as p approaches zero, the formula (15) relating the adhesive strength to applied force becomes

$$F = \left(\sum_{m=1}^{M} \frac{\chi^{(m)}}{D^{(m)}} \right) \frac{D_1 G}{1 - \cos(\theta_p)}. \tag{24}$$

We conclude that the maximum peel force is given at the instant that the stiffest segment is at the peel front and

$$F_{\text{Het}} = \max_j \{D^{(j)}\} \left(\sum_{m=1}^{M} \frac{\chi^{(m)}}{D^{(m)}} \right) \frac{G}{1 - \cos(\theta_p)} = \max_j \{D^{(j)}\} \left(\sum_{m=1}^{M} \frac{\chi^{(m)}}{D^{(m)}} \right) F_{\text{hom}}. \tag{25}$$

We recognize

$$D_e = \left(\sum_{m=1}^{M} \frac{\chi^{(m)}}{D^{(m)}} \right)^{-1},$$

the harmonic mean of the rigidities, to be the effective bending rigidity of the heterogeneous film. Therefore, the above result states that the effective peeling force required to peel a periodic tape with small period is the same as the force required to peel a two-segment film consisting of a stiff portion with rigidity $D_1 = \max_j \{D^{(j)}\}$ and a compliant portion of rigidity $D_2 = D_e$. Since the period is small compared to the region that is bent, one sees only the effective bending energy.

Since the largest rigidity is greater than the harmonic mean of the various rigidities, the prefactor above is larger than unity. So, we do indeed have an enhancement over the homogeneous case.

Finally, for a two-segment unit cell with $D^{(1)} \geq D^{(2)}$, the result Eq. (25) above reduces to

$$F_{\text{Het}}^{\text{sp}} = \left[\chi^{(1)} + \chi^{(2)} \frac{D^{(1)}}{D^{(2)}} \right] \frac{G}{1 - \cos(\theta_p)} \approx \chi^{(2)} \frac{D^{(1)}}{D^{(2)}} F_{\text{hom}} \tag{26}$$

for large concentration of compliant constitute ($\chi^{(2)} \gg \chi^{(1)}$) or high level of heterogeneity ($D^{(1)} \gg D^{(2)}$).

2.3.2. Large period ($p \gg \sqrt{D_e/2G}$)

Note that as the period p goes to infinity, the length of the segments do the same. Consider a situation where the first interface s_1 is just emerging from the peeled region. We can use an argument similar to that in Section 2.2 to show that $\theta_2 \to \theta_p$ as $p/\sqrt{D_e/2G} \to \infty$. In other words, this case reduces to the two-segment film with D_1 and D_2 to be the rigidities of the segments closest to the peel front. We conclude that the maximum peel force is given by

$$F_{\text{Het}} = \max_j \left(\frac{D_j}{D_{j+1}} \right) \frac{G}{1 - \cos(\theta_p)} = \max_j \left(\frac{D_j}{D_{j+1}} \right) F_{\text{hom}}, \tag{27}$$

where the formula is interpreted cyclically. When the period becomes large, the bending zone is limited to two adjacent segments, and thus the film behaves like a two-segment film. Further the ratio of rigidities is clearly greater than unity and thus we have an enhancement relative to the homogeneous case.

For a two-segment unit cell with $D^{(1)} \geq D^{(2)}$, the result Eq. (27) above reduces to

$$F_{\text{Het}}^{\text{lp}} = \frac{D^{(1)}}{D^{(2)}} F_{\text{hom}}. \tag{28}$$

This agrees with the two-segment tape Eq. (23). Further, comparing to the case of the small period, Eq. (26), we see that the enhancement in the case of large period is independent of volume fraction and is larger.

The result (27) also shows an interesting possibility for multi-segment tape. Suppose we peel the same multi-segment tape analyzed above from the other end. Then the peel front approaches the various segments in the opposite sequence, and thus the maximum peel force is given by

$$F_{\text{Het}} = \max_j \left(\frac{D_j}{D_{j-1}} \right) \frac{G}{1 - \cos(\theta_p)} = \max_j \left(\frac{D_j}{D_{j-1}} \right) F_{\text{hom}}. \tag{29}$$

Since it is possible that $\max_j(D_j/D_{j+1}) \neq \max_j(D_j/D_{j-1})$ (e.g., a three-segment tape with $D_i = 1,2,3$, $\max_j(D_j/D_{j+1}) = 3$ while $\max_j(D_j/D_{j-1}) = 2$), the maximum peel force peeling one way can be different from that peeling the other way. In other

words, heterogeneity can give rise to *asymmetry* in the peeling force. We will explore asymmetry in the context of patterning the adhesive surface in the subsequent work (Xia et al., 2012a).

2.4. General case

For a general situation where the position $s_1, \ldots, s_N$ is given, we employ the following numerical method to solve the non-linear equations (15) and (18):

1. Make an initial guess $\{\theta_i\} = \{\theta_1, \theta_2, \ldots, \theta_N\}$.
2. Estimate F from the current set of $\{\theta_i\}$ using Eq. (15).
3. Starting from $k=1$ and going till $k=N$, we obtain θ_k from $\theta_1, \theta_2, \ldots, \theta_{k-1}$ using Eq. (18).
4. Re-calculate F with the new set of θ_k. Check the relative error between the previous and current values of F. If the error is smaller than a user-defined threshold, terminate the iteration. Otherwise, go to step 2.

After a final set of θ_i ($1 \leq i \leq N$) is obtained, we numerically evaluate the displacement at the end of the film using Eq. (3).

On occasion, we will seek to understand the history of the peel force and displacement as the peel progresses. We do so starting with an initial set of positions $\{s_i\}$ and then incrementing them while computing the peel force and displacement at each step.

3. Experiment

3.1. Model material system

A series of experiments have been performed and compared with the theoretical predictions. For direct comparison between the theoretical and experimental results, an ideal experimental model system should possess constant film/substrate adhesion energy as well as well-controlled heterogeneity in film bending stiffness. This consideration led to the design of a simple composite film structure, as illustrated in Fig. 2(a). The base of the composite film was a thin polyester (PET) sheet. To introduce heterogeneity in bending stiffness, an array of PET stiffeners of uniform thickness was bonded onto the base using UV curable glue. The level of the heterogeneity could be manipulated over a wide range by varying the thickness of the stiffeners. The flat side of the film was applied to a thick epoxy layer (Devon, 2Ton® clear epoxy) rigidly supported on a plastic substrate, while the epoxy was still wet. The epoxy was then allowed to fully cure for 16 h at ambient conditions, before a peel test was carried out to peel off the composite film from the epoxy layer. The elastic modulus and Poisson's ratio of polyester were determined to be 3.8 GPa and 0.42, respectively, by performing uniaxial tensile tests. The reduced modulus of the UV curable glue was evaluated by instrumented nanoindentation to be about 4 MPa, which was three orders of magnitude lower than that of polyester, and was therefore neglected in the calculation of composite bending stiffness. The intrinsic adhesion energy of the polyester–epoxy interface was measured by 90-degree peel testing to be 5.1 J/m². The geometric parameters of the composite film were: width of the composite film $w=38.0$ mm, thickness of the base film $t_1=0.161$ mm, thickness of the UV curable glue $t_2=0.010$–0.030 mm, thickness of the stiffeners $t_3=0.025$–0.161 mm, length of the stiffeners $l=6$–10 mm, and center-to-center spacing of the stiffeners $p=12$–20 mm. This set of parameters gave a range of bending rigidity ratio of stiff (with stiffeners) to compliant (without stiffeners) regions from 2.0 to 8.8.
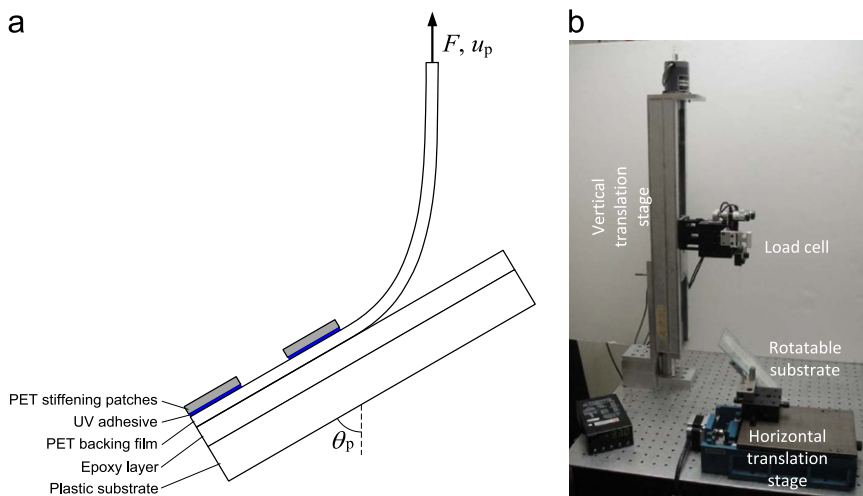
Fig. 2. (a) Schematic image of the experimental setup showing the composite film and loading geometry. (b) Photograph of the peel test setup.

3.2. Peel test setup

The commonly used peel test configuration was employed to measure peel forces required to peel off a composite film at various peel angles. As shown in Fig. 2(b), the free end of the composite film was peeled off at a constant speed, v_p, and a peel angle, θ_p, from the flat epoxy layer. For ease of experimental implementation, the film was always peeled upwards with a vertically aligned motorized linear translation stage, and the plastic substrate was rotated about its hinge to obtain any desired peel angle. Further, the peel angle was kept constant by translating the substrate in the horizontal direction at a speed of $v_h = v_p \sin \theta_p / (1 - \cos \theta_p)$ with a second motorized translation stage. The corresponding peel force is measured by a load cell with 500 g load capacity.

4. Results

4.1. Representative peeling response

Fig. 3 shows the experimentally measured steady-state peeling force as a function of the displacement at a peel angle of 90° for a heterogeneous film consisting of alternating stiff and compliant segments and compares it with that of two homogeneous films, one uniformly stiff and another uniformly compliant. The measured response of the two homogeneous films overlap with each other in agreement with Eq. (21), the well-known result of Rivlin (1944). However, the response of the heterogeneous film is extremely different. The figure starts when the peel front is in the compliant region. It increases dramatically as the stiff region approaches the peel front and rises to a peak as the peel front coincides with the interface between the peeled compliant region and unpeeled stiff region. The force drops suddenly as the peel front passes the stiff region, and the cycle repeats with each period. The force required to peel a macroscopic length of the film is equal to the peak force, and this is significantly higher compared to that of the homogeneous films. This is as anticipated by the theory presented earlier. Henceforth, we normalize the peeling force using that of the homogeneous films.

Fig. 4(a) and (b) shows the transient response of two films with different heterogeneity ratios ($D_s/D_c = 2.0$ and 8.8) being peeled starting from a compliant region and proceeding to alternating stiff and compliant regions. Notice that for both films the peaks are initially larger approaching that of the case of a two-segment film and then gradually level off to a steady state value. Fig. 4(a) and (b) also compares the experimental measurement with the predicted theoretical response computed with the general algorithm described in Section 2.4. The theoretical curves are parametrized by the position of the peel front. As the peel front traverses the compliant region, the peel force increases reaching a peak at the compliant to stiff interface. Note that the rising portion of the theoretical and experimental curves as well as the trends of the peaks compare well with the experiment. The experimental peaks are slightly lower than the theoretical peaks for $D_s/D_c = 8.8$ and this is to be expected due to the occurrence of plastic deformation as well as shearing between the base film and stiffeners at very large peel force.

The theoretical curves show a snap-back phenomenon: as the peel front passes the stiff-to-compliant interface (for both films) or the compliant-to-stiff interface (for $D_s/D_c = 8.8$), the peeling displacement decreases. In other words, there
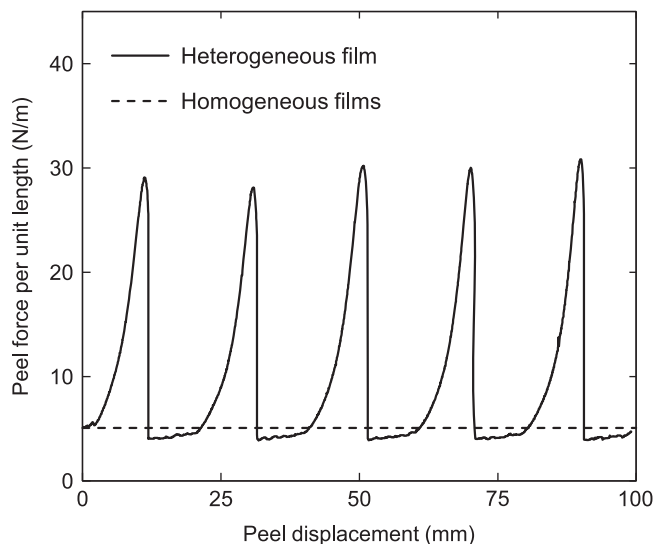
Fig. 3. Experimental steady-state peel force vs. displacement curves of a heterogeneous film consisting of alternating stiff and compliant segments as well as two homogeneous films, one uniformly stiff and one uniformly compliant. The measured response of the two homogeneous films overlaps with each other.
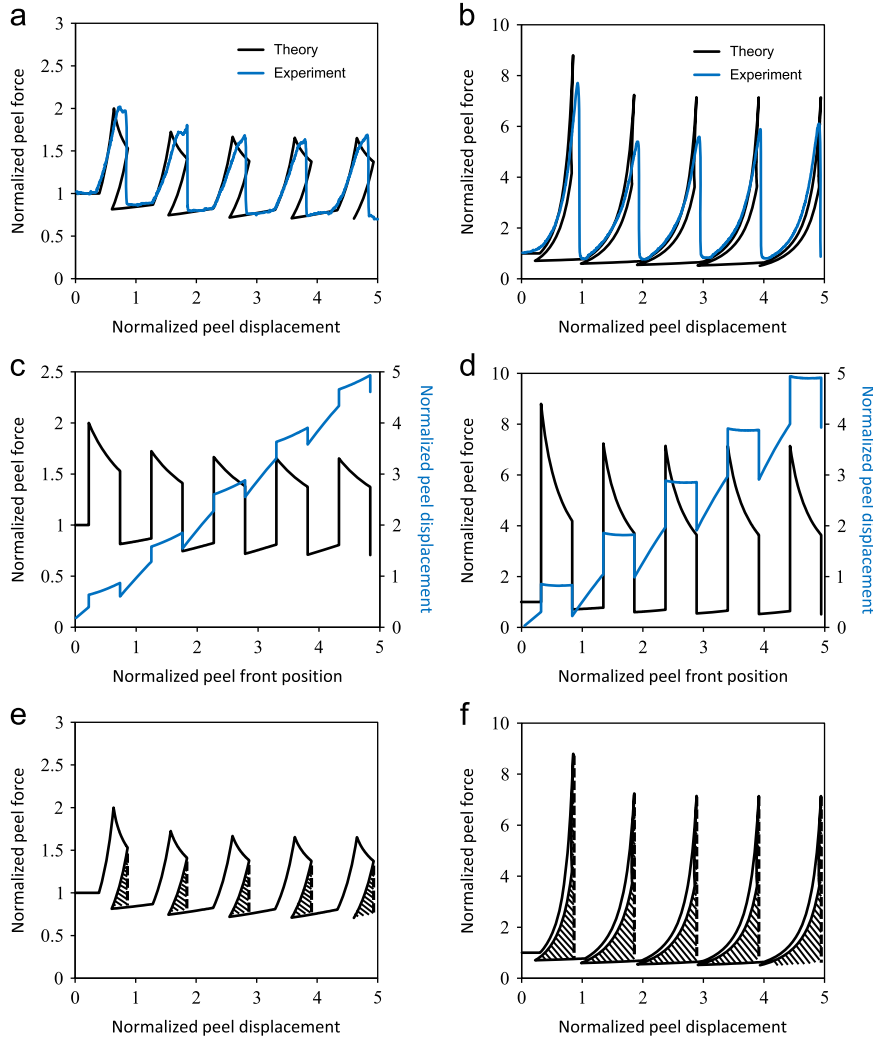
Fig. 4. (a), (b) Comparison between theoretical and experimental peel force–displacement curves for $D_s/D_c=2.0$, $p/\sqrt{D_e/2G}=0.89$ and $D_s/D_c=8.8$, $p/\sqrt{D_e/2G}=0.77$. (c), (d) Theoretical peel force and peel displacement as a function of peel front position corresponding to (a) and (b). (e), (f) Theoretical peel force under peel-front control and displacement control corresponding to (a) and (b). The other parameters are $\chi_s=0.5$ and $\theta_p=90°$.

are two equilibrium forces compatible for a given peel displacement and vice-versa. This snap-back is illustrated in Fig. 4(c) and (d) which plots both the peel force and peel displacement as a function of the peel front position. This snap-back is not observed in the experiment because these are carried out at prescribed displacement. Fig. 4(e) and (f) compares the peel force for both displacement control and peel-front position control. The hatched area is the difference between the two, and may be regarded as the energy that is dissipated due to the snap-back instability. The applied force has to supply this work in addition to the work of adhesion. Therefore, we define a *quasi-static (q.s.) work of peeling*

$$G_{het}^{qs} = G + \frac{\text{energy dissipated due to snap-back in one period}}{\text{period}}. \tag{30}$$

4.2. Effect of contrast in heterogeneity

The calculated values of the normalized steady-state (s.s) peak peel force for one set of geometrical parameters are shown in Fig. 5(a) against the ratio of D_s to D_c. Also shown is a linear curve with slope one (dashed line), which represents the theoretical enhancement of either a tape with two segments (and hence equal to that of the first peak) or a tape with infinite period, $F_{het}^{2seg}/F_{hom} = F_{het}^{lp}/F_{hom} = D_s/D_c$. The steady-state peel strength is lower than the initial strength, due to stiffening of the peeled-off region. However, an approximately linear relationship appears to hold for large contrast.

The steady-state enhancement in the quasi-static work of peeling is an order of magnitude lower than that in peel strength, but nevertheless still quite considerable, as shown in Fig. 5(b). As the level of heterogeneity increases, the
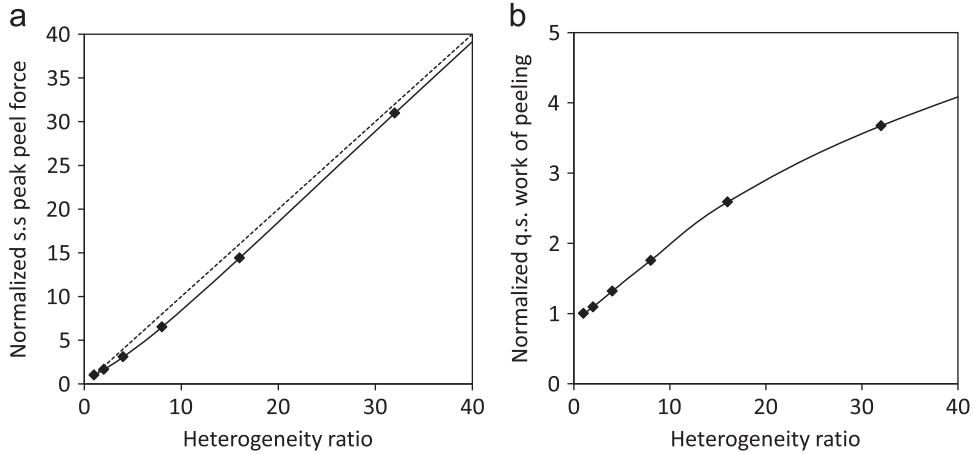
Fig. 5. Effect of contrast. Calculated values of the steady-state: (a) Normalized peak peel force, $F_{\text{het}}/F_{\text{hom}}$. (b) Normalized quasi-static work of peeling $G_{\text{het}}^{\text{qs}}/G$ as a function of level of heterogeneity, D_s/D_c. The other parameters are $p/\sqrt{D_e/2G}=0.8$, $\chi_s=0.5$, and $\theta_p=90°$. The symbols are the computed values and the solids lines are a guide to the eye. The dashed line in (a) is the value for a two-segment tape or an infinite period tape, $F_{\text{het}}^{\text{2seg}}/F_{\text{hom}} = F_{\text{het}}^{\text{lp}}/F_{\text{hom}} = D_s/D_c$.
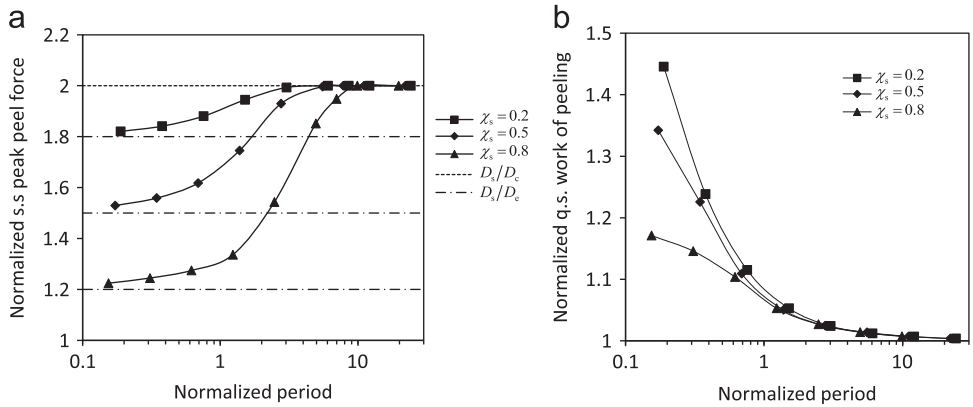
Fig. 6. Effect of length scale. Calculated values of the steady-state: (a) Normalized peak peel force, $F_{\text{het}}/F_{\text{hom}}$. (b) Normalized quasi-static work of peeling $G_{\text{het}}^{\text{qs}}/G$ as a function of normalized period $p/\sqrt{D_e/2G}$ for three length fractions. The other parameters are $D_s/D_c=2$ and $\theta_p=90°$. The symbols are the computed values and the solids lines are a guide to the eye. The asymptotic value for large period $F_{\text{het}}^{\text{sp}}/F_{\text{hom}}$ is indicated by a dashed line, and the asymptotic values for small period $F_{\text{het}}^{\text{sp}}/F_{\text{hom}}$ are indicated by dash-dotted lines.

enhancement factor of the quasi-static work of peeling continues to increase without an apparent limit, with a slower increasing rate at higher level of heterogeneity.

4.3. Effect of length scale of heterogeneity

Fig. 6(a) shows the calculated values of the steady-state normalized peak peel force as a function of the normalized period for three different length fractions of stiff material. Note that for each length fraction, the curves interpolate between the limiting values $F_{\text{het}}^{\text{sp}}/F_{\text{hom}}$ (which depends on length fraction) at small period and $F_{\text{het}}^{\text{lp}}/F_{\text{hom}}$ (which is independent of length fraction) at large period.

The enhancement in the quasi-static work of peeling has an opposite dependence on the period of heterogeneity, as shown in Fig. 6(b). In particular, the quasi-static work of peeling goes to zero at a rate of $1/p$ with large period. This is because the energy dissipated due to snap-back in one period saturates and thus goes to zero at a rate of $1/p$ when normalized with period (cf. Eq. (30)).

4.4. Effect of peel angle

In the Section 2.3, we have shown that the normalized peel force required to peel off a two-component heterogeneous film is independent of peel angle for both small and large periods. This is confirmed by the computed values shown in Fig. 7(a). The latter is also confirmed by a comparison of theory and experiment in Fig. 8. However, Fig. 7(a) also shows that the normalized peel force does indeed depend on the peel angle for intermediate periods. The effect of peel angle on the
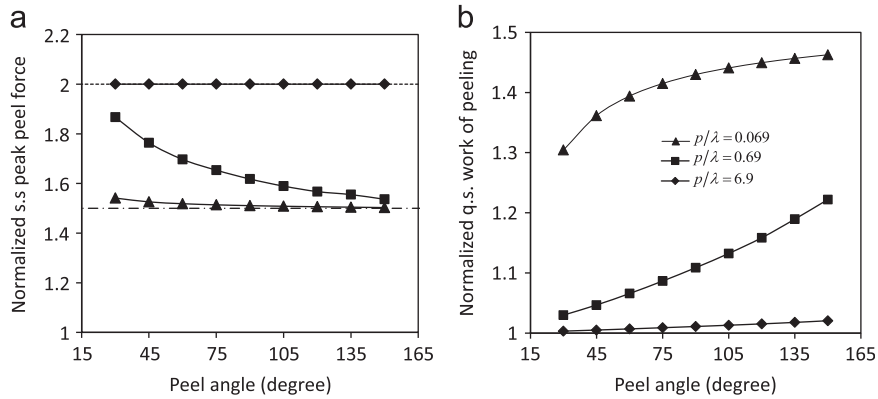
Fig. 7. Effect of peel angle. Calculated values of the steady state: (a) Normalized peak peel force, F_{het}/F_{hom}. (b) Normalized quasi-static work of peeling G_{het}^{qs}/G as a function of peel angle for three different periods. The other parameters are $D_s/D_c = 2$ and $\chi_s = 0.5$. The symbols are the computed values and the solids lines are a guide to the eye. The asymptotic value for large period F_{het}^{lp}/F_{hom} is indicated by a dashed line, and the asymptotic value for small period F_{het}^{sp}/F_{hom} is indicated by a dash-dotted line.
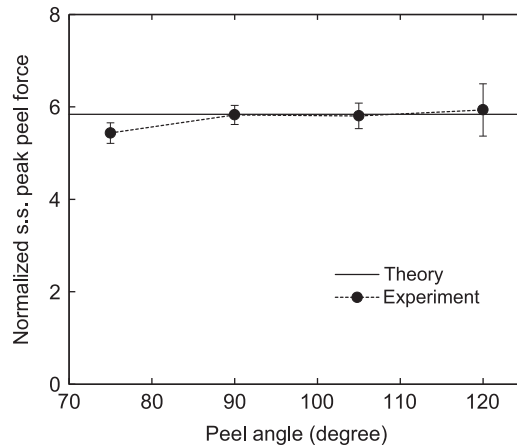
Fig. 8. Comparison of effect of peel angle between theory and experiment. Here, $D_s/D_c = 5.8$, $p/\sqrt{D_e/2G} = 1.6$, and $\chi_s = 0.5$.

quasi-static work of peeling is examined in Fig. 7(b). This is essentially angle dependent for all cases, with diminishing enhancement at low peel angles.

5. Discussion

We have demonstrated that the adhesion strength of a thin film can be substantially improved through the introduction of heterogeneity in its elastic bending rigidity with absolutely *no* change in the actual adhesive interface. The physical origin of adhesion enhancement is clear from both the experiment and the model. The peel force enhancement is due to rapid variation in stored elastic energy as the peel front crosses from a compliant to a stiff region. A significant portion of the work done by the peel force goes into bending of the suddenly stiffer region, thereby giving rise to a drop in the total driving force and a peak in the peel force when a constant peel velocity is imposed. On the other hand, the enhancement in work of peeling is a consequence of energy dissipation associated with the snap-back instability in peel force–displacement curves.

A variety of ways can be employed to create the desired heterogeneity. Since the bending rigidity depends on the third power of the film thickness, it is most effective to modulate the thickness. In this study, we have worked on a model system that has a patterned, laminated composite structure. Other possible methods to introduce heterogeneity include, but not limited to, modulating spatial distribution of film thickness, and patterning elastic modulus by masked irradiation if the film material is irradiation-sensitive. There is no upper limit of enhancement with increasing degree of heterogeneity. However, the actual level of enhancement may be bounded by various practical factors, such as plasticity and strength of the film material.

The level of enhancement depends sensitively on the length scale of heterogeneity. The enhancement in the force required to peel the adhesive is largest when the length scale of heterogeneity is extremely large compared to the characteristic length of bending of the film. The enhancement decreases with decreasing length scale, but does not completely vanish even in this

limit. In other words, one always sees the heterogeneity no matter how small it is. We note that this observation has to be tempered with the observation that in this work the adhesive process is assumed to be completely 'brittle' with an infinitesimal process zone. In some material systems like the common pressure sensitive systems (e.g., the Scotch[®] adhesive tape), the size of process zone is not negligible compared to the characteristic length of bending. In such situations, our results would be limited to scales which are large compared to the size of the process zone. Thus, our small-scale asymptotic limit may not be attainable.

In this work, we largely framed the discussion in terms of the force required to peel a macroscopic length of film. However, it is common to describe adhesion in terms of energy density based on the work required to peel an adhesive film. This would be equal to the area under the force–displacement curve shown in Fig. 3, for example. Clearly, this enhancement is smaller than the enhancement in the peeling force (they would be equal if the force were uniformly at the peak). Thus, in a heterogeneous system, the relation between force and energy does not directly hold. However, notice that the actual force–displacement curve would likely be rate-dependent (even if the material were rate-independent) due to the waves that would emanate as the peel front traverses the stiff/compliant interface. Thus we expect the effective work of peeling to be significantly rate-dependent, and to increase monotonically with peeling rate. Thus, a lower bound is the quasi-static work of peeling defined in Eq. (30). We see from Fig. 6, for example, that $G_{\text{het}}^{\text{qs}}/G < F_{\text{het}}/F_{\text{hom}}$ as expected. However, notice from this figure that $G_{\text{het}}^{\text{qs}}/G \rightarrow F_{\text{het}}/F_{\text{hom}}$ as the length scale becomes very small.

We have limited ourselves to a one-dimensional situation by considering the striped geometry. This allowed us to analyze the problem using a (modified) Euler–Bernoulli beam theory. However, the striped geometry gives rise to a highly anisotropic situation. When tested along the parallel direction, the film is not expected to exhibit any adhesion enhancement. The process of peeling in this case is uniform, and can be therefore described by the Rivlin model as for a homogeneous film. To achieve enhancement in all directions, it is necessary to incorporate two-dimensional patterns, arranged in a deterministic or random way. A theoretical analysis would require plate theory, and evolution equations for the peel front line. We investigate this in the context of adhesive heterogeneity in subsequent parts of this work (Xia et al., 2012a; Ponson and Xia, 2012).

We have assumed the film is inextensible and only considered its bending. For thin films made of soft materials that are peeled at very low angles, the effect of extensibility may be important (Kendall, 1975b). We address this in the context of adhesive heterogeneity in subsequent parts of this work (Ponson and Xia, 2012).

While we consider adhesion of a thin film, the significance of our results extends beyond, since we may regard adhesion fronts as a prototypical problem in condensed matter physics. We anticipate similar effects of heterogeneity on brittle fracture (Rice, 1985; Legrand et al., 2011), dislocations (Hirth and Lothe, 1992), phase boundaries (Dondl and Bhattacharya, 2010), and wetting fronts (Joanny and de Gennes, 1984). Most of the research effort on heterogeneities has focused on the disordered case where G is described by a quenched noise, resulting in universal features through intermittent dynamics and scale-invariant roughening (Bonamy and Bouchaud, 2011; Sethna et al., 2001). Our work shows that there is much to gain in terms of overall properties by studying the deterministic and periodic cases. Specifically we anticipate that in many of these phenomena, patterning the elastic modulus would produce strong drops of the driving force resulting in largely enhanced resistance. This can potentially open the door to engineering new materials where the toughness, strength, etc., can be tuned through designed defects.

Acknowledgments

Appendix A

To find the limiting form of Eq. (15) for a periodically heterogeneous film as the period p tends to zero, we notice that the denominator

$$\sum_{i=1}^{\infty} D_i f(\theta_i, \theta_{i-1}) = \sum_{k=0}^{\infty} \sum_{j=1}^{M} D^{(j)}[\cos(\theta^{(k,j)} - \theta_{\text{p}}) - \cos(\theta^{(k,j-1)} - \theta_{\text{p}})] = \sum_{k=0}^{\infty} \sum_{j=1}^{M} D^{(j)} \sin(\theta_{\text{p}} - \theta^{(k,0)})\Delta\theta^{(k,j)} + O(p^2), \quad \text{(A.1)}$$

where we used Taylor expansion to get from the first line to the second. To proceed further, we seek to relate the change of angle in the different segments of the unit cell to the overall change of angle within one unit cell and to the volume fraction of the segment. To that end, we recall the moment continuity condition (8) and approximate the derivatives of inclination angle with finite difference formulas. This leads to

$$D^{(j+1)}\theta'\big|_{s^{(k,j)+}} - D^{(j)}\theta'\big|_{s^{(k,j)-}} = \frac{D^{(j+1)}\Delta\theta^{(k,j+1)}}{p\chi^{(j+1)}} - \frac{D^{(j)}\Delta\theta^{(k,j)}}{p\chi^{(j)}} + O(p) = 0. \quad \text{(A.2)}$$

The above equation implies

$$\frac{D^{(m)}\Delta\theta^{(k,m)}}{\chi^{(m)}} = \frac{D^{(j)}\Delta\theta^{(k,j)}}{\chi^{(j)}} + O(p^2) \quad \text{for any } m,j \in [1,M]$$

and therefore

$$\Delta\theta^{(k,m)} = \frac{D^{(j)}\Delta\theta^{(k,j)}\chi^{(m)}}{\chi^{(j)}D^{(m)}} + O(p^2). \tag{A.3}$$

Summing over m from 1 to M, we get

$$\sum_{m=1}^{M}\Delta\theta^{(k,m)} = \theta^{(k,M)} - \theta^{(k,0)} = \Delta\theta^{(k)} = \frac{D^{(j)}\Delta\theta^{(k,j)}}{\chi^{(j)}}\sum_{m=1}^{M}\frac{\chi^{(m)}}{D^{(m)}} + O(p^2) \tag{A.4}$$

or

$$D^{(j)}\Delta\theta^{(k,j)} = \Delta\theta^{(k)}\chi^{(j)}\left(\sum_{m=1}^{M}\frac{\chi^{(m)}}{D^{(m)}}\right)^{-1} + O(p^2). \tag{A.5}$$

Substituting this back into Eq. (A.1), we obtain

$$\sum_{i=1}^{\infty} D_i f(\theta_i,\theta_{i-1}) = \left(\sum_{m=1}^{M}\frac{\chi^{(m)}}{D^{(m)}}\right)^{-1}\sum_{k=1}^{\infty}\sin(\theta_{\mathrm{p}}-\theta^{(k,0)})\Delta\theta^{(k)} + O(p^2). \tag{A.6}$$

We now let $p \to 0$ and notice that since $\Delta\theta \to 0$, the sum becomes an integral. We conclude that

$$\sum_{i=1}^{\infty} D_i f(\theta_i,\theta_{i-1}) \to \left(\sum_{m=1}^{M}\frac{\chi^{(m)}}{D^{(m)}}\right)^{-1}\int_0^{\theta_{\mathrm{p}}}\sin(\theta_{\mathrm{p}}-\theta)\,d\theta = \left(\sum_{m=1}^{M}\frac{\chi^{(m)}}{D^{(m)}}\right)^{-1}(1-\cos\theta_{\mathrm{p}}). \tag{A.7}$$

We can now obtain the instantaneous peel force by substituting this into Eq. (15)

$$F = \left(\sum_{m=1}^{M}\frac{\chi^{(m)}}{D^{(m)}}\right)\frac{D_1 G}{1-\cos(\theta_{\mathrm{p}})}. \tag{A.8}$$

References

Barthelat, F., Espinosa, H.D., 2007. An experimental investigation of deformation and fracture of nacre-mother of pearl. Exp. Mech. 47 (3), 311–324.
Bonamy, D., Bouchaud, E., 2011. Failure of heterogeneous materials: a dynamic phase transition?. Phys. Rep. 498 (1), 1–44.
Bonamy, D., Santucci, S., Ponson, L., 2008. Crackling dynamics in material failure as the signature of a self-organized dynamic phase transition. Phys. Rev. Lett. 101 (4), 045501.
Bouchaud, E., 1997. Scaling properties of cracks. J. Phys. Condens. Matter. 9 (21), 4319–4344.
Bower, A.F., Ortiz, M., 1991. A 3-dimensional analysis of crack trapping and bridging by tough particles. J. Mech. Phys. Solids 39 (6), 815–858.
Bower, A.F., Ortiz, M., 1993. The influence of grain-size on the toughness of monolithic ceramics. J. Eng. Mater. Technol. ASME 115, 228–236.
Chan, E.P., Ahn, D., Crosby, A.J., 2007. Adhesion of patterned reactive interfaces. J. Adhes. 83 (5), 473–489.
Chen, B., Shi, X.H., Gao, H.J., 2008. Apparent fracture/adhesion energy of interfaces with periodic cohesive interactions. Proc. R. Soc. A 464 (35), 657–671.
Chen, B., Wu, P.D., Gao, H.J., 2009. Geometry- and velocity-constrained cohesive zones and mixed mode fracture/adhesion energy with periodic cohesive interactions. Proc. R. Soc. A 465 (35), 1043–1053.
Chung, J.Y., Chaudhury, M.K., 2005. Roles of discontinuities in bio-inspired adhesive pads. J. R. Soc. Interface 2 (2), 55–61.
Cox, B., Yang, Q.D., 2006. In quest of virtual tests for structural composites. Science 314 (5802), 1102–1107.
Dalmas, D., Barthel, E., Vandembroucq, D., 2009. Crack front pinning by design in planar heterogeneous interfaces. J. Mech. Phys. Solids 57 (3), 446–457.
Dondl, P.W., Bhattacharya, K., 2010. A sharp interface model for the propagation of martensitic phase boundaries. Arch. Ration. Mech. Anal. 197, 599–617.
Evans, A.G., Hutchinson, J.W., 1989. Effects of non-planarity on the mixed-mode fracture-resistance of bimaterial interfaces. Acta Metall. 37 (3), 909–916.
Fowkes, F.M., 1987. Role of acid-base interfacial bonding in adhesion. J. Adhes. Sci. Technol. 1, 7–27.
Ghatak, A., Mahadevan, L., Chung, J.Y., Chaudhury, M.K., Shenoy, V., 2004. Peeling from a biomimetically patterned thin elastic film. Proc. R. Soc. A Math. Phys. 460 (2049), 2725–2735.
Guduru, P.R., 2007. Detachment of a rigid solid from an elastic wavy surface: theory. J. Mech. Phys. Solids 55 (3), 445–472.
Guduru, P.R., Bull, C., 2007. Detachment of a rigid solid from an elastic wavy surface: experiments. J. Mech. Phys. Solids 55 (3), 473–488.
Hirsch, E.H., Varga, I.K., 1978. The effect of ion irradiation on the adherence of germanium films. Thin Solid Films 52, 445–452.
Hirth, J.P., Lothe, J., 1992. Theory of Dislocations. Krieger Publishing Company.
Hudaa, M.S., Drzala, L.T., Mohantyb, A.K., Misra, M., 2008. Effect of fiber surface-treatments on the properties of laminated biocomposites from poly(lactic acid) (PLA) and kenaf fibers. Compos. Sci. Technol. 68, 424–432.
Hutchinson, J.W., Suo, Z., 1992. Mixed-mode cracking in layered materials. Adv. Appl. Mech. 29, 63–191.
Joanny, J.F., de Gennes, P.G., 1984. A model for contact angle hysteresis. J. Chem. Phys. 81, 552–562.
Kendall, K., 1975a. Control of cracks by interfaces in composites. Proc. R. Soc. Lond. A 341 (1627), 409–428.
Kendall, K., 1975b. Thin-film peeling—elastic term. J. Phys. D Appl. Phys. 8 (13), 1449–1452.
Legrand, L., Patinet, S., Leblond, J.B., Frelat, J., Lazarus, V., Vandembroucq, D., 2011. Coplanar perturbation of a crack lying on the mid-plane of a plate. Int. J. Fract. 170, 67–82.
Li, Q.Y., Kim, K.S., 2009. Micromechanics of rough surface adhesion: a homogenized projection method. Acta Mech. Solida Sin. 22 (5, (special issue SI)), 377–390.
Liu, Q., Wijn, J.R., Bakker, D., Blitterswijk, C.A., 1996. Surface modification of hydroxyapatite to introduce interfacial bonding with polyactive^{TM} 70/30 in a biodegradable composite. J. Mater. Sci. Mater. Med. 7, 551–557.

Menig, R., Meyers, M.H., Meyers, M.A., Vecchio, K.S., 2000. Quasi-static and dynamic mechanical response of haliotis rufescens (abalone) shells. Acta Mater. 48 (9), 2383–2398.

Milton, G.W., 2002. The Theory of Composites. Cambridge University Press.

Nemat-Nasser, S., Hori, M., 1999. Micromechanics: Overall Properties of Heterogeneous Materials. North-Holland.

Ponson, L., Bonamy, D., 2010. Crack propagation in brittle heterogeneous solids: material disorder and crack dynamics. Int. J. Fract. 162 (1–2), 21–31.

Ponson, L., Xia, S. M. Adhesion of heterogeneous thin films: 3. Adhesive heterogeneity at shallow angles of peel, in preparation.

Ramrus, D.A., Berg, J.C., 2006. Enhancement of adhesion to heterogeneously patterned substrates. Colloid. Surf. A 273 (1–3), 84–89.

Reedy, E.D., 2008. Effect of patterned nanoscale interfacial roughness on interfacial toughness: a finite element analysis. J. Mater. Res. 23 (11), 3056–3065.

Rice, J.R., 1985. 1st-order variation in elastic fields due to variation in location of a planar crack front. J. Appl. Mech. Technol. ASME 52 (3), 571–579.

Rivlin, R.S., 1944. The effective work of adhesion. Paint Technol. 9, 215.

Sethna, J.P., Dahmen, K.A., Myers, C.R., 2001. Crackling noise. Nature 410, 242–250.

Xia, S.M., Ponson, L., Ravichandran, G., Bhattacharya, K. Adhesion of heterogeneous thin films: 2. Adhesive heterogeneity at large angles of peel, in preparation.

Xia, S.M., Ponson, L., Ravichandran, G., Bhattacharya, K., 2012b. Toughening and asymmetry in peeling of heterogeneous adhesives. Phys. Rev. Lett. 108, 196101.

Xu, G., Bower, A.F., Ortiz, M., 1998. The influence of crack trapping on the toughness of fiber reinforced composites. J. Mech. Phys. Solids 46, 1815–1833.

Zavattieri, P.D., Hector, L.G., Bower, A.F., 2007. Determination of the effective mode-I toughness of a sinusoidal interface between two elastic solids. Int. J. Fract. 145 (3), 167–180.